Emission Factors and Optical Properties of Black and Brown Carbon Emitted at a Mixed-Conifer Forest Prescribed Burn

Supporting Information

James D.A. Butler,[1,2*] Afsara Tasnia,[3] Deep Sengupta,[4] Nathan Kreisberg,[5] Kelley C. Barsanti,[3,6] Allen H. Goldstein,[1,4] Chelsea V. Preble,[1,2] Rebecca A. Sugrue,[1,2] Thomas W. Kirchstetter[1,2]

[1]Department of Civil and Environmental Engineering, University of California, Berkeley, Berkeley, California 94720

[2]Energy Technologies Area, Lawrence Berkeley National Laboratory, Berkeley, California 94720

[3]Department of Chemical and Environmental Engineering, Center for Environmental Research and Technology, University of California, Riverside, Riverside, California 92507

[4]Department of Environmental Science, Policy, and Management, University of California, Berkeley, Berkeley, California 94720

[5]Aerosol Dynamics Inc., Berkeley, California 94720

[6] Atmospheric Chemistry Observations and Modeling, U.S. National Science Foundation National Center for Atmospheric Research, Boulder, Colorado 80301

*Corresponding author email: twkirchstetter@lbl.gov

Number of Pages: 16

Number of Tables: 2

Number of Figures: 11

Methods

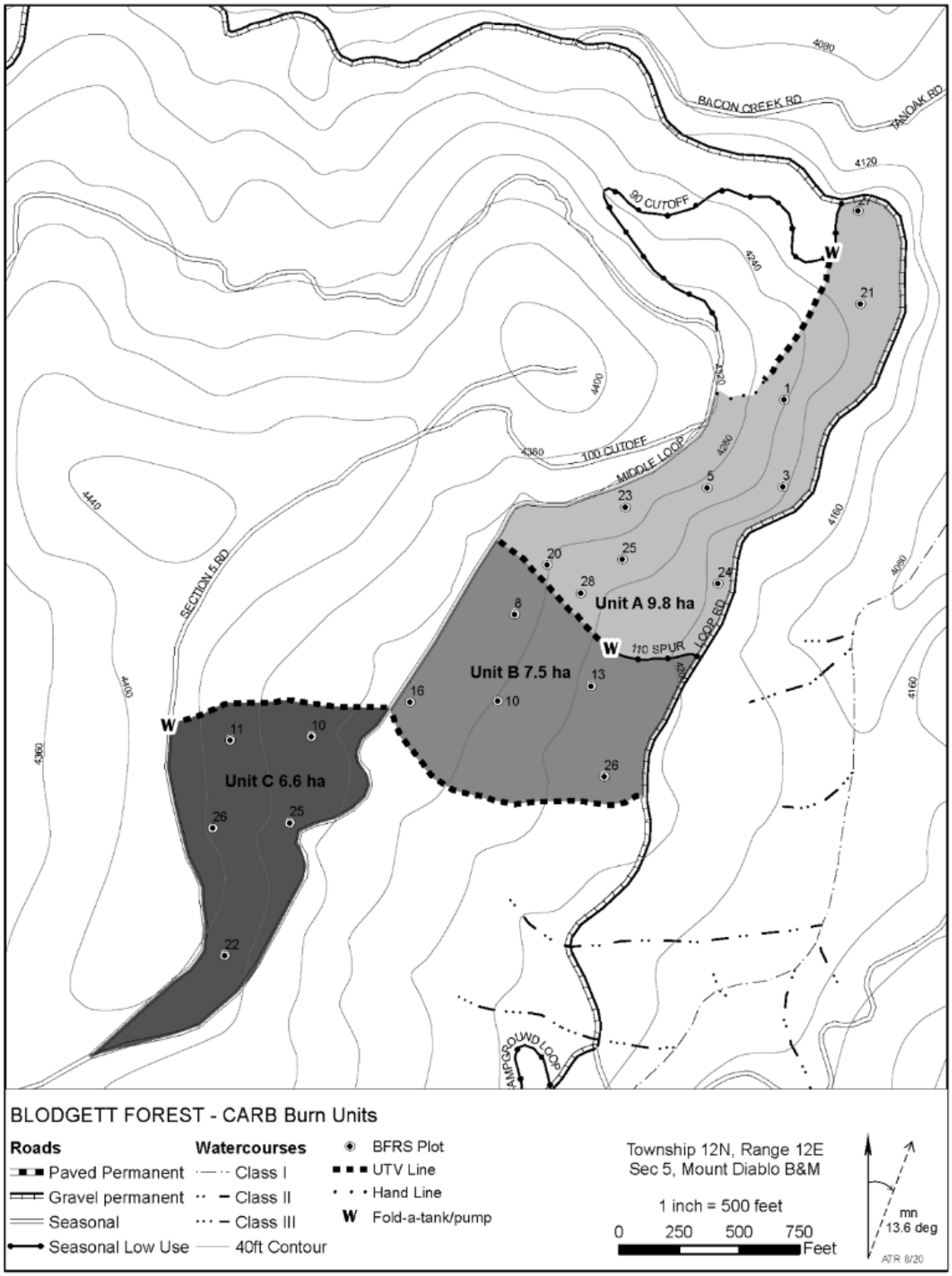

Figure S1: Three units (labeled A, B, C with area noted) treated by prescribed burns at the Blodgett Forest Research Station. Unit A was burned on Days 1 and 2, Unit B on Day 3, Unit C on Day 4.

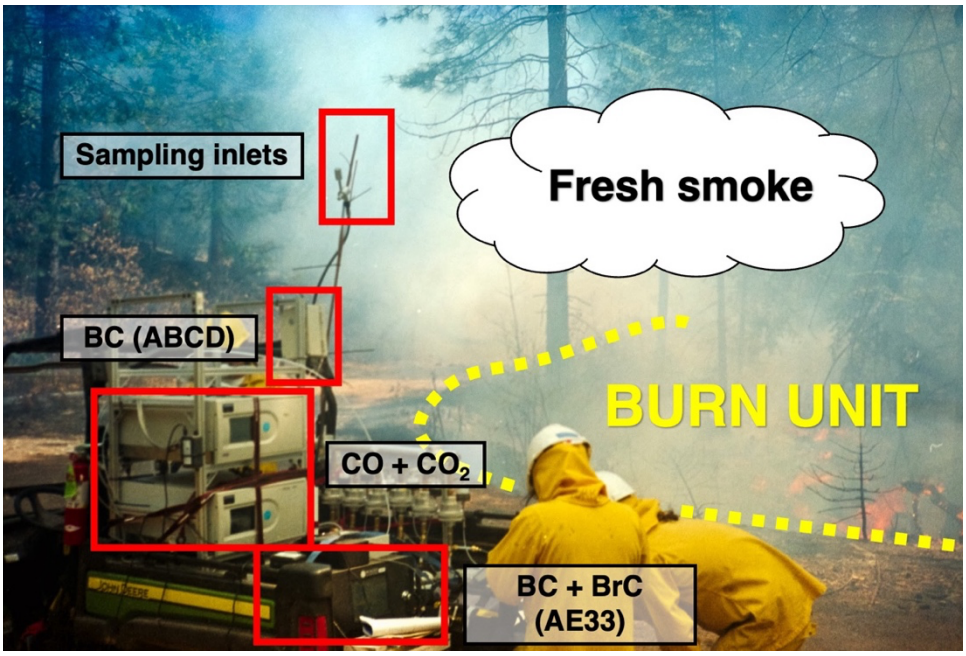

Figure S2: Ground sampling platform setup on the utility task vehicle with the mounted filter-based photometers and gas analyzers. Sampling inlet shown attached above the roll cage of the UTV.

Data Quality Assurance and Control. Field data were post-processed for quality assurance and quality control before analysis, as described in detail below: (1) datasets from each instrument were time aligned on a 1 Hz time basis; (2) BC measurements were adjusted to account for the filter loading artifact; and (3) timeseries plots of gases and particle concentrations were visually inspected for data quality.

(1) Timestamp Alignment. To calculate an emission factor (EF) on any time basis, pollutant timeseries and/or peaks needed to be integrated together across analyzers on a synchronized time basis. During field sampling, passing plumes of smoke would cause each analyzer to record a peak in concentration at timestamps that varied by ±60 seconds. This misalignment of the BrC (AE33), BC (AE33 and ABCD), CO, and CO_2 1 Hz concentration data on the ground platform was due to variations in analyzer internal clocks and differences in response times of the filter-based photometers and gas analyzers. To remedy this issue and reduce uncertainty in EF integration calculations, a timestamp alignment routine was performed on the AE33 BC dataset, ABCD BC dataset, and CO dataset against the CO_2 dataset.

The combustion of fuels in the prescribed burn was the only major source of BC, BrC, CO, and CO_2 during field measurements, so the pollutants measured in the sampled smoke

plumes were assumed to be co-emitted and linearly correlated. The Pearson correlation coefficient (ρ) was used to determine the appropriate timestamp offset for each analyzer, as it is a measure of linear correlation between two normally distributed random variables (Schober et al., 2018). These timestamp adjustments were made to the AE33 BC, ABCD BC, and CO datasets. The BrC dataset were not included in the analysis, since its timestamps were identical to the AE33 BC dataset; the AE33 BC timestamp adjustment was applied to the BrC timestamp, too.

The alignment routine was written as a *Python* function with *pearsonr* statistical function in the *scipy* library. For each unaligned pollutant dataset, timestamps were artificially offset between -120 to +120 seconds and then ρ was calculated between the unaligned datasets (AE33 BC, ABCD BC, & CO) to the CO_2 dataset, as presented in Figure S3. The resulting distribution of calculated ρ for each unaligned pollutant dataset all displayed smooth function within the range of applied timestamp offsets. The timestamp offset for each pollutant was chosen where ρ was maximized. The final adjusted timestamps were offset by –2, +51, and +54 seconds for CO, AE33 BC, and ABCD BC, respectively.

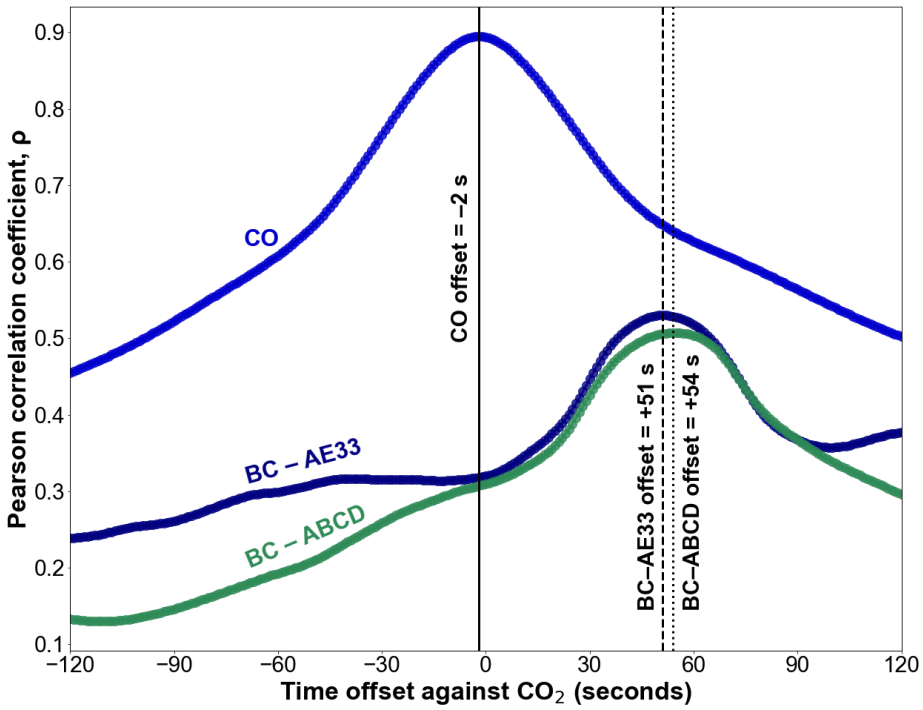

Figure S3: Pearson correlation coefficient (ρ) of CO, BC AE33, and BC ABCD datasets against CO_2 dataset for a range of timestamp offsets (±120 seconds). Maximum ρ for each unaligned dataset (marked with a vertical line) corresponds to the chosen timestamp offset of –2, +51, and +54 seconds for the CO, BC–AE33, and BC–ABCD datasets, respectively.

(2) BC Loading Artifact Compensation. BC datasets were first filtered using the ordinary least squares (OLS) linear regression calculated from the *statsmodels* library in Python (Josef Perktold et al., 2024). Following prior work, BC concentrations greater than 100 μg m^{-3} and less than the mean absolute error (MAE) on a 1-minute averaging basis were excluded from the dataset (Caubel et al., 2019):

$$MAE = \frac{\sum_{t_i}^{t_n} |BC(t)|}{n}$$

The MAE is a measure of measurement noise and was calculated from background sampling when prescribed burn smoke was not present (Table S1). On a 1-minute average time-basis, all coefficients of determination for the OLS regression between the AE33 and ABCD were 0.81–0.85.

Table S1: Mean absolute error (MAE) (μg m^{-3}) of aethalometers during background sampling.

Average time-basis	**Multiwavelength aethalometer (AE33)**	**Lower-cost BC sensor (ABCD)**
1 second (not averaged)	0.4	2.8
10 second	0.2	0.5
1 minute	0.1	0.2

Filter-based aerosol absorption photometers become less sensitive to aerosol light absorption with increasing aerosol deposition, which results in an underestimation of BC concentration. This is known as the BC loading artifiact (Jimenez et al., 2007). The AE33 has a real-time loading artifact correction algorithm that corrects raw BC concentrations by comparing the optical attenuation through two filter spots loaded at different flow rates (Drinovec et al., 2015). Co-location of the ABCD and AE33 provided the basis to apply a source-specific loading artifact correction to the ABCD BC dataset. For the ABCD BC dataset, data was post-processed following the method outlined in Caubel et al. (2019), including removing BC concentrations measured when ATN levels exceeded a value of 100.

The ABCD BC dataset was adjusted for its loading artifact using Equation S1, where the compensation parameter, *a*, was applied to uncompensated BC concentrations as a function of measured ATN:

$$BC_{ABCD,compensated} = \frac{BC_{ABCD,uncompensated}}{a \cdot \exp\left(-\frac{ATN}{100}\right) + (1-a)} \quad \text{(Equation S1)}$$

The source-specific value for *a* was determined by minimizing the difference between 1-minute averaged uncompensated ABCD BC data regressed against averaged auto-compensated AE33 BC data (Figure S4). The optimal compensation parameter of $a = 0.5$ resulted in the regression slope closest to unity (Figure S5).

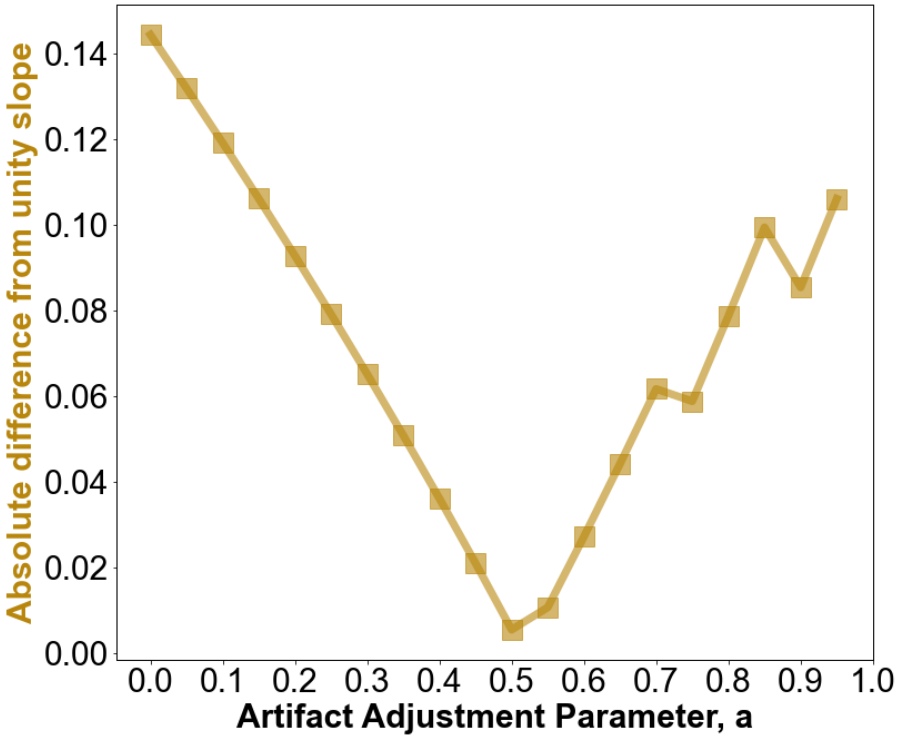

Figure S4: Difference in linear regression slopes from unity of 1-minute averaged ABCD BC dataset, compensated by *a*, against the AE33 BC dataset.

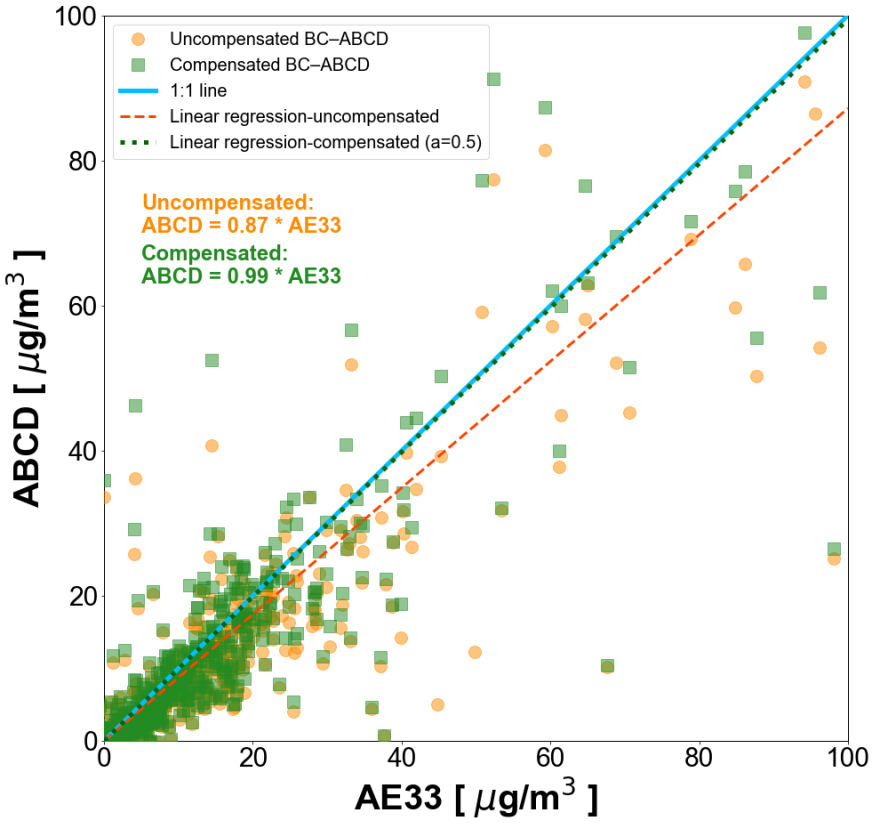

Figure S5: Averaged 1-minute AE33 BC (x-axis) versus ABCD BC (y-axis) before (orange circles) and after (green squares) application of loading artifact compensation. Linear regression slopes displayed, with the compensated slope nearly identical to the unity slope.

(3) Visual Inspection. Timeseries plots were generated for 1-minute AE33 BC and ABCD BC concentrations across the four days of prescribed burns and are presented in Figure S6. Similarly, 1-minute excess CO and CO_2 mixing ratios are presented in Figure S7. Excess CO and CO_2 were calculated after subtracting the background concentrations listed in Table S2. For CO, the background concentration was assumed to be zero, as no other sources of incomplete combustion were present at the burn. The CO_2 background concentration was determined daily before the start of the burn for both the ground and aerial sampling platforms. Visual inspection of pollutant timeseries in both Figures S6 and S7 revealed near background concentrations of pollutants during the morning sample session on Day 4, noted in Figures S6 and S7 as having "Unfavorable sampling conditions". No emission factors or optical properties were computed during this period.

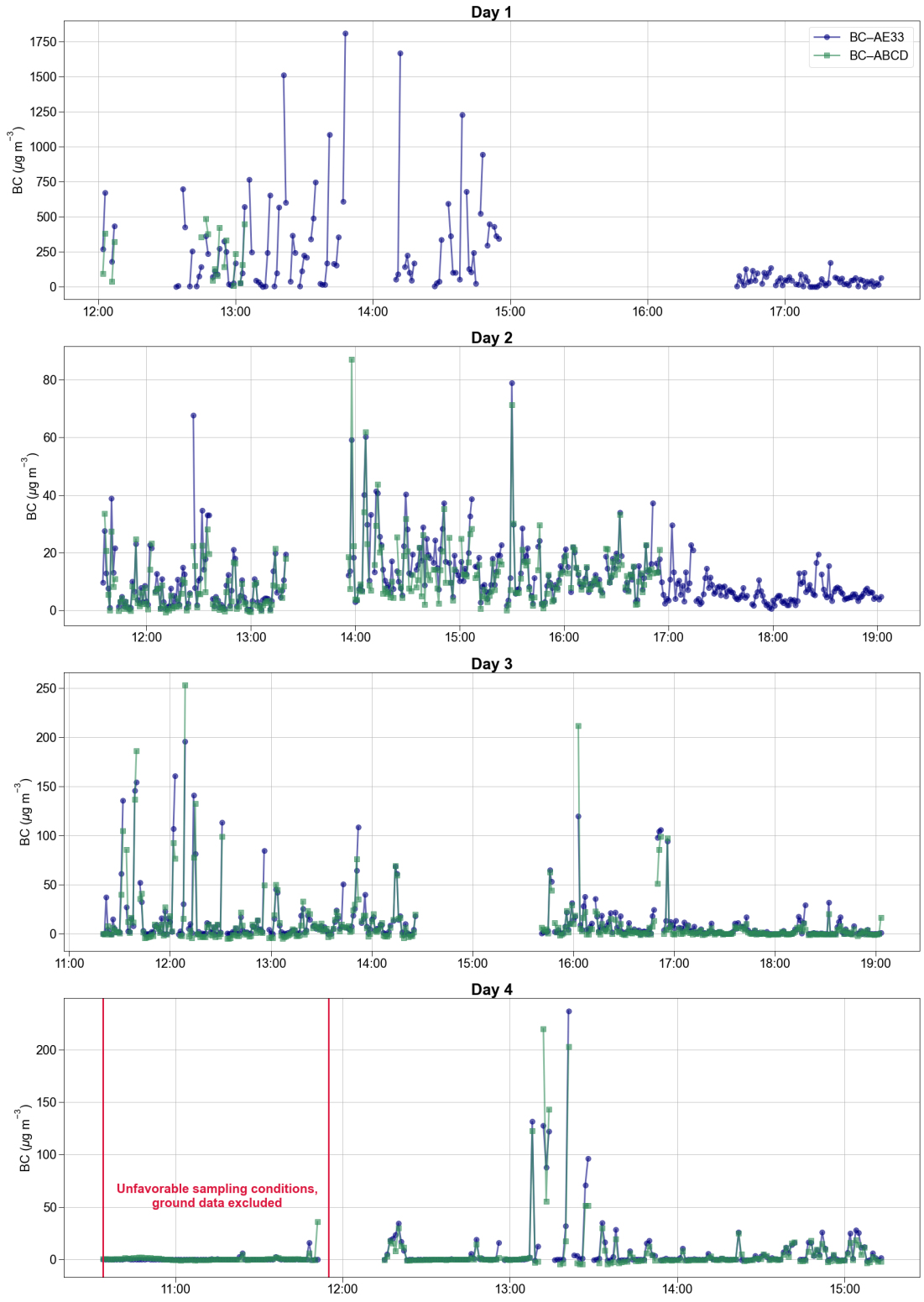

Figure S6: Timeseries of 1-minute averaged BC concentrations measured by the AE33 and ABCD for each of the four burn days.

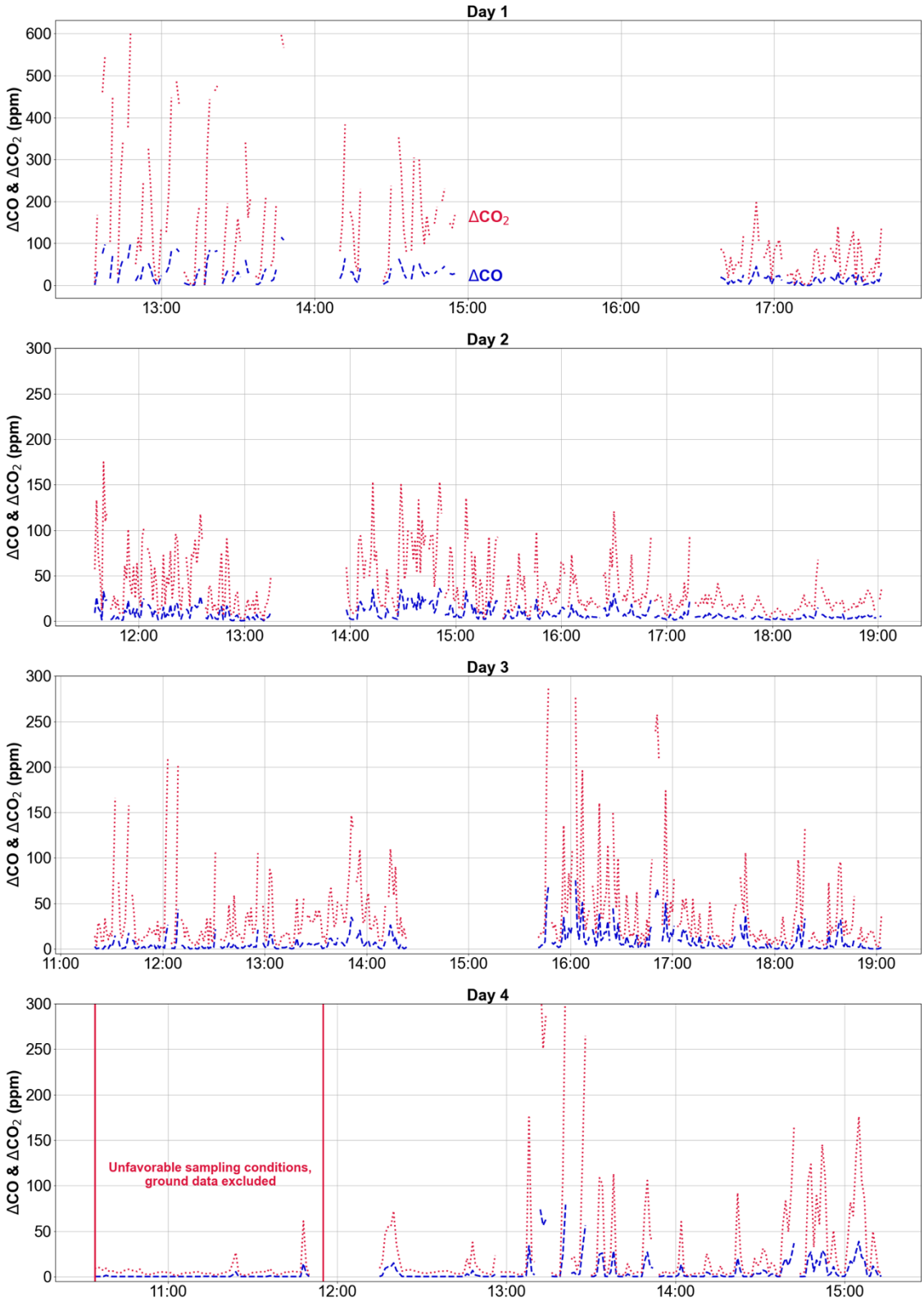

Figure S7: Timeseries of 1-minute averaged excess CO and CO_2, along with modified combustion efficiency (MCE) on the secondary y-axis for each of the four burn days.

Table S2: Background CO and CO_2 concentrations for each day of prescribed burns

Day	Ground CO [ppm]	Ground CO_2 [ppm]	Aerial CO [ppm]	Aerial CO_2 [ppm]
1	0	409	0	420
2	0	410	0	420
3	0	404	0	420
4	0	402	0	420

Temporal Basis of Emission Factors. From top to bottom in left panel of Figure S8, ground BC emission factors were determined using three different approaches: (1) 1-minute, 5-minute, and 10-minute integration windows subsampled from the continuous dataset, shown in the top panel in green; (2) an ATN cycle basis (i.e., one aethalometer filter tape advancement), shown in the middle panel in orange; and (3) a sampling location basis, shown in grey in the bottom panel. The average and median emission factor across the subsample time bases in the top panel were nearly equal, with an absolute difference of ~0.01 and ~0.03 g kg^{-1}, respectively. All three subsample distributions underestimated the sampling location average of 0.40 g kg^{-1} that is shown in the bottom panel by 0.1 g kg^{-1}. The ATN cycle emission factor distribution had the greatest average and median values, which exceeded the sampling location by a factor of 1.6 and 1.3, respectively. Air quality modeling frameworks use a measure of central tendency, such as an average, as the representative emission factor for a prescribed burn event in emissions inventories and exposure estimates. By varying the time basis by which emission factors were calculated, we demonstrate that the average emission factor and shape of each distribution is sensitive to the chosen integration time basis.

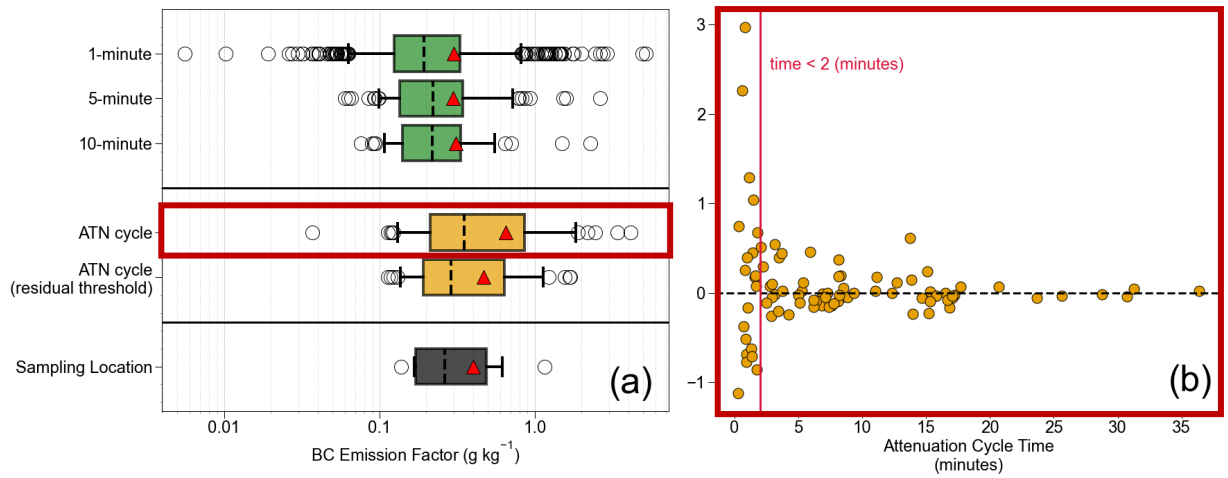

Figure S8: (a) BC emission factor distributions calculated on the ground platform by three subsampled time bases (1, 5, and 10 minutes – green boxes), the ATN cycle (orange boxes), and by the sampling location basis (gray box). Boxes represent the interquartile range and tails the 5th and 95th percentile. The median is provided as the dashed line, the average as a triangle, and individual values beyond the 5th and 95th percentile whiskers as open circles. Note the logarithmic scale on the x-axis. (b) BC emission factor residual difference between the ATN cycle and the sampling location bases plotted against ATN cycle time (minutes) for the ground platform aethalometer. A residual threshold of 2 minutes is plotted as a vertical line and used in the lower boxplot in the middle panel of (a).

The sampling location emission factor distribution (n = 9) on the bottom row of the left panel in Figure S8 is likely the most representative of the prescribed burn. This temporal basis captured long periods of the event at a fixed location, integrated of all measurement data minutes, and was consistent with the methodology in previous field studies (Aurell et al., 2021; Strand et al., 2015). In this work, the minimum sampling location period of 27 minutes was greater than 95% of ATN cycle times. While this temporal basis may be most representative of the burn event, it produces the least number of samples and is the least temporally resolved.

A greater the number of samples in a field study allows for the investigation of combustion condition dependence and variability within each combustion regime like the analyses in Figures 1 and 2. The subsampled emission factors produced the greatest number of samples and were the most temporally resolved; however, this temporal basis underestimated the sampling location average because many emission factors were calculated during minimal smoke capture periods, between passing peaks in concentration, like those shown in Figures S6 and S7. This effect was pronounced for the most temporally resolved 1-minute emission factors, which

were the only distribution to span two orders of magnitude and have values less than 0.03 g kg^{-1} (Figure S8). During minimal smoke capture periods, pollutant concentrations were still elevated, and an emission factor could be calculated. Nevertheless, the bulk of smoke blew away from the ground sampling platform during these minimal smoke capture periods, as shown in Figure S9. Any emission factors computed during these windows were likely not representative of the burn event.

Figure S9: Prescribed burn of Unit C on the morning of Day 4, with ground sampling platform ~10 m (left) and 20 m (right) directly behind the viewer.

The temporal basis of the emissions factors calculated on the ATN cycle was variable, with a range of 1–36 minutes. Given the limitations of highly temporally resolved emission factors, residual differences of the ATN cycle and sampling location emission factors are plotted against the ATN cycle time in the right panel of Figure S8. Emission factors calculated during the ATN cycle times less than 2 minutes tended to have highest residual values (i.e., greater than 1 g kg^{-1}), as demarcated by the vertical line in Figure S8. These emission factors were calculated during the highest concentration period of the study, when BC > 250 μg m^{-3}. High BC concentration, and thus a high aerosol loading rate, caused the aethalometer to reach its ATN limit quickly, often before the entire plume of smoke could be measured and before the aethalometer and gas analyzers could return to near-background concentration. Instead, the aethalometer measurements were interrupted by a filter tape advancement and integration of a passing peak in concentration was truncated causing a high residual and unrepresentative emission factor.

When a 2-minute ATN cycle residual threshold was applied, the ATN cycle average BC emission factor was 0.47 g kg^{-1}, which was closest to the sampling location average when compared to the raw ATN cycle and subsample distributions in Figure 4. The residual threshold ATN cycle distribution exhibited the most similar shape to the sampling location distribution, as depicted in the bottom two rows of Figure S8. The residual threshold ATN cycle emission factors also maintained a wider range of MCE values (0.77–0.93) than the sampling location basis (0.79–0.87) that included values in the flaming combustion phase, which supplemented the flaming phase aerial platform emission factors. Retaining field samples on both platforms under flaming and smoldering conditions ensured combustion-phase average emission factors in Figure 2 were representative of ground-level and aloft smoke.

Results and Discussion

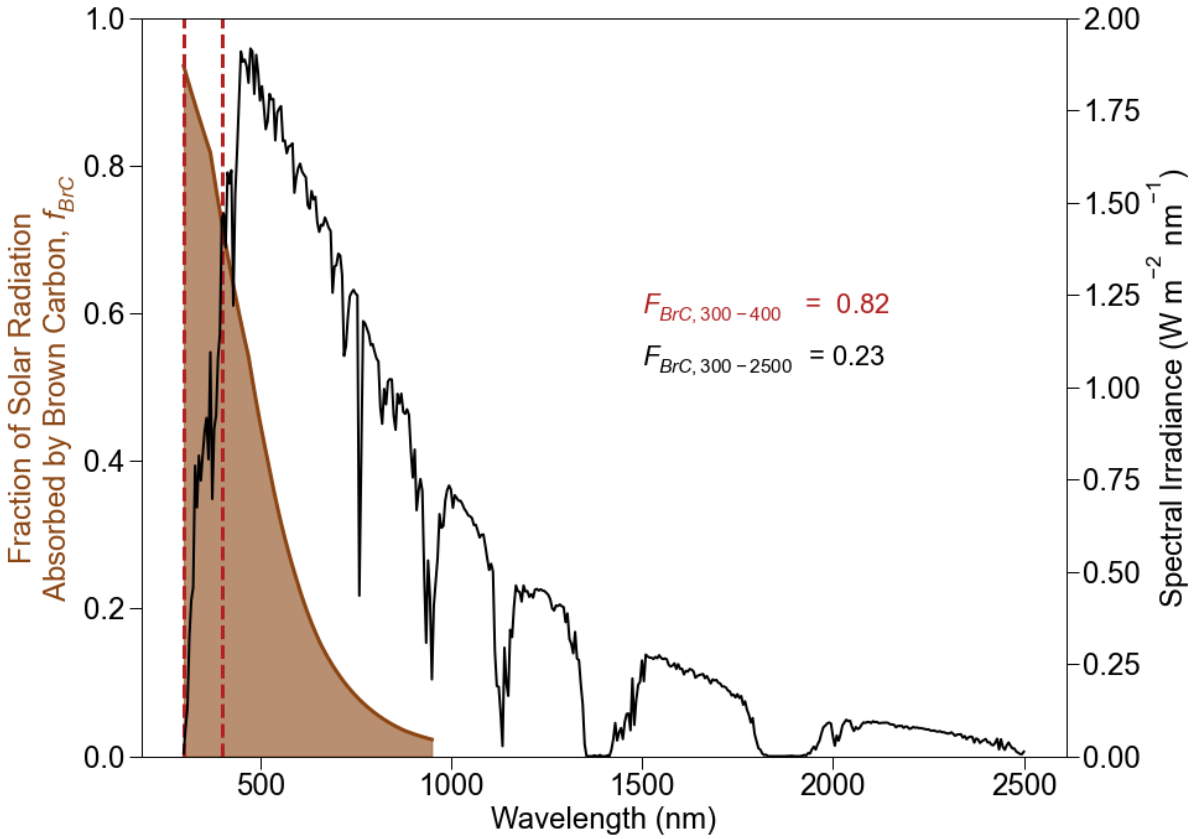

Figure S10: Estimated fraction of solar radiation absorbed by brown carbon (left primary y-axis) and Air Mass 1 Global Horizontal (AM1GH) spectral irradiance from Levinson et al. (2010) (right y-axis) plotted as a function of wavelength (x-axis).(Levinson et al., 2010) Integrated fractions of solar radiation absorbed by brown carbon in the UV region (300–400 nm) and full spectrum (300–2500 nm) noted.

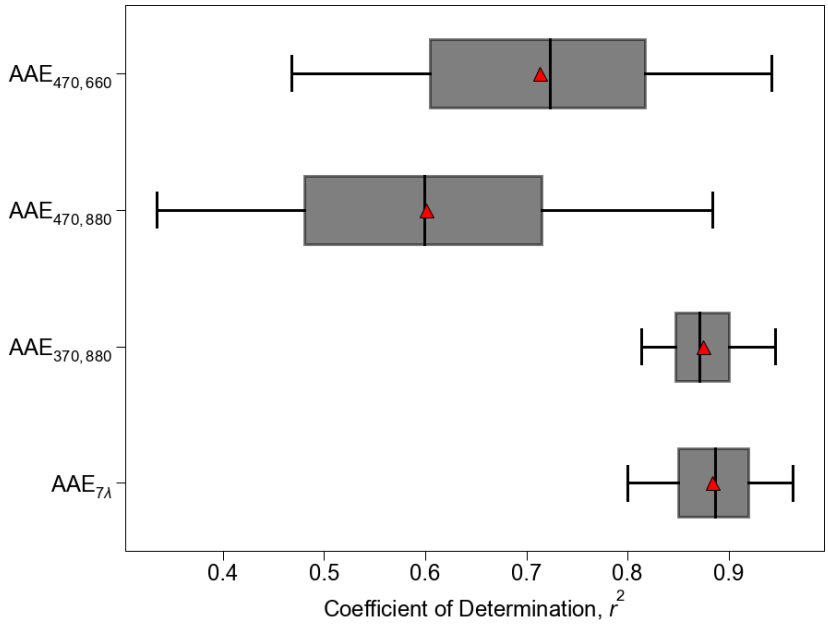

Figure S11: Coefficient of determination (r^2) for predicted absorption values calculated from power law fit AAEs listed along the y-axis of the figure.

References

Aurell, J., Gullett, B., Holder, A., Kiros, F., Mitchell, W., Watts, A., and Ottmar, R.: Wildland fire emission sampling at Fishlake National Forest, Utah using an unmanned aircraft system, Atmos. Environ., 247, 118193, https://doi.org/10.1016/j.atmosenv.2021.118193, 2021.

Caubel, J. J., Cados, T. E., Preble, C. V., and Kirchstetter, T. W.: A Distributed Network of 100 Black Carbon Sensors for 100 Days of Air Quality Monitoring in West Oakland, California, Environ. Sci. Technol., 53, 7564–7573, 2019.

Drinovec, L., Močnik, G., Zotter, P., Prévôt, A. S. H., Ruckstuhl, C., Coz, E., Rupakheti, M., Sciare, J., Müller, T., Wiedensohler, A., and Hansen, A. D. A.: The "dual-spot" Aethalometer: an improved measurement of aerosol black carbon with real-time loading compensation, Atmospheric Meas. Tech., 8, 1965–1979, https://doi.org/10.5194/amt-8-1965-2015, 2015.

Jimenez, J., Claiborn, C., Larson, T., Gould, T., Kirchstetter, T. W., and Gundel, L.: Loading Effect Correction for Real-Time Aethalometer Measurements of Fresh Diesel Soot, J. Air Waste Manag. Assoc., 57, 868–873, https://doi.org/10.3155/1047-3289.57.7.868, 2007.

Josef Perktold, Skipper Seabold, Kevin Sheppard, ChadFulton, Kerby Shedden, jbrockmendel, j-grana6, Peter Quackenbush, Vincent Arel-Bundock, Wes McKinney, Ian Langmore, Bart Baker, Ralf Gommers, yogabonito, s-scherrer, Yauhen Zhurko, Matthew Brett, Enrico Giampieri, yl565, Jarrod Millman, Paul Hobson, Vincent, Pamphile Roy, Tom Augspurger, tvanzyl, alexbrc, Tyler Hartley, Fernando Perez, Yuji Tamiya, and Yaroslav Halchenko: statsmodels/statsmodels: Release 0.14.2, , https://doi.org/10.5281/ZENODO.593847, 2024.

Levinson, R., Akbari, H., and Berdahl, P.: Measuring solar reflectance—Part I: Defining a metric that accurately predicts solar heat gain, Sol. Energy, 84, 1717–1744, https://doi.org/10.1016/j.solener.2010.04.018, 2010.

Schober, P., Boer, C., and Schwarte, L. A.: Correlation Coefficients: Appropriate Use and Interpretation, Anesth. Analg., 126, 1763, https://doi.org/10.1213/ANE.0000000000002864, 2018.

Strand, T., Gullett, B., Urbanski, S., O'Neill, S., Potter, B., Aurell, J., Holder, A., Larkin, N., Moore, M., and Rorig, M.: Grassland and forest understorey biomass emissions from prescribed fires in the south-eastern United States – RxCADRE 2012, Int. J. Wildland Fire, 25, 102–113, https://doi.org/10.1071/WF14166, 2015.